Electronic Supplementary Informations

For

Syntheses, crystal structures and steady state and time-resolved fluorescence properties of a PET based macrocycle and its dinuclear $Zn^{II}/Cd^{II}/Hg^{II}$ complexes

Leena Mandal, Samit Majumder and Sasankasekhar Mohanta*

Table S1 Spectral parameters of spectrophotometric titrations of H_2L with $ZnCl_2$, $Cd(NO_3)_2 \cdot 4H_2O$, $\{Hg(NO_3)_2 \cdot H_2O + NaCl\}$ and $Hg(OAc)_2$

	λ_{max} (nm) [ε (M^{-1} cm^{-1})]			
H_2L	–	231 (sh) [12,411]	286 [5,623]	–
1	206 [82,146]	250 [19,057]	294 [8113]	–
H_2L+$ZnCl_2$ (saturated spectrum at 1:2.2 equivalent ratio)	204 [89,652]	249 [17,481]	293 [7,748]	–
2	–	267 (sh) [8,567]	294 [9,592]	–
H_2L+$Cd(NO_3)_2 \cdot 4H_2O$(saturated spectrum at 1:2.2 equivalent ratio)	–	253 (sh) [7,475]	291 [8,890]	–
3	–	–	304 [6,156]	362 [2,529]
H_2L+ $\{Hg(NO_3)_2$ + NaCl} (saturated spectrum at 1:2.4 equivalent ratio)	–	–	291 [5,604]	359 [2,345]
H_2L+ $Hg(OAc)_2$ (saturated spectrum at 1:2.0 equivalent ratio)	–	241 [33,926]	304 [7,454]	359 [3,509]

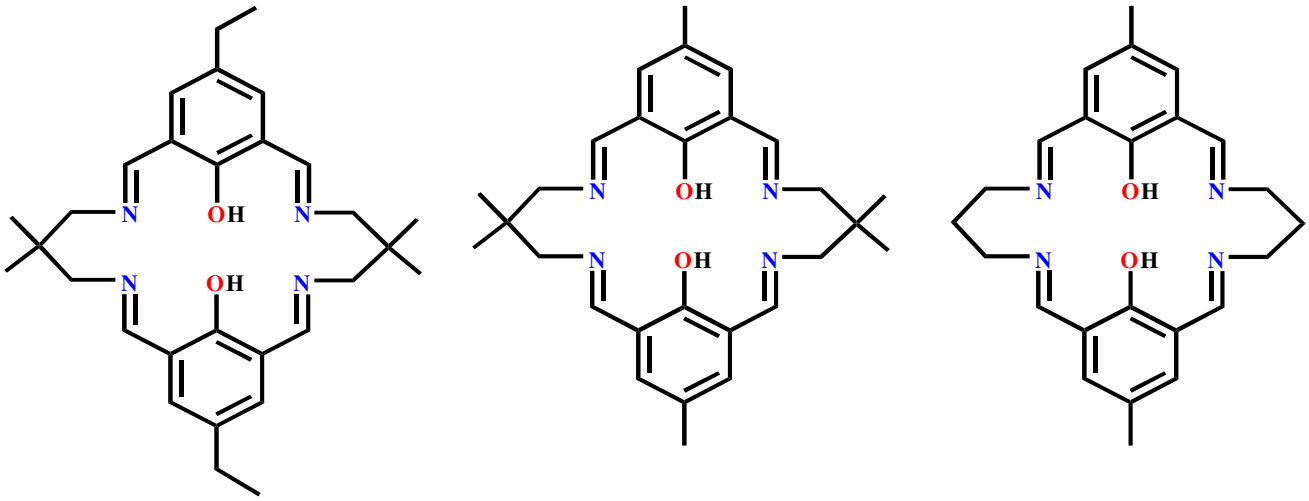

H_2L^1 H_2L^2 H_2L^3

Scheme S1 Chemical structures of ligands.

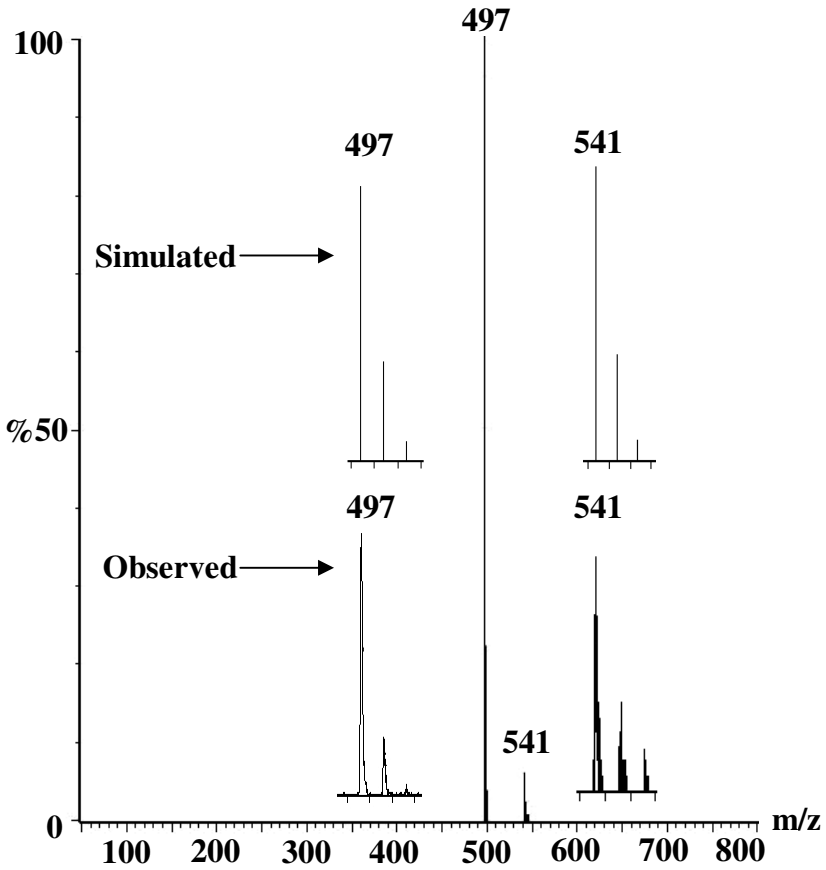

Fig. S1 Electrospray ionization mass spectrum positive (ESI-MS positive) of H_2L in acetonitrile, showing observed and simulated isotopic distribution patterns.

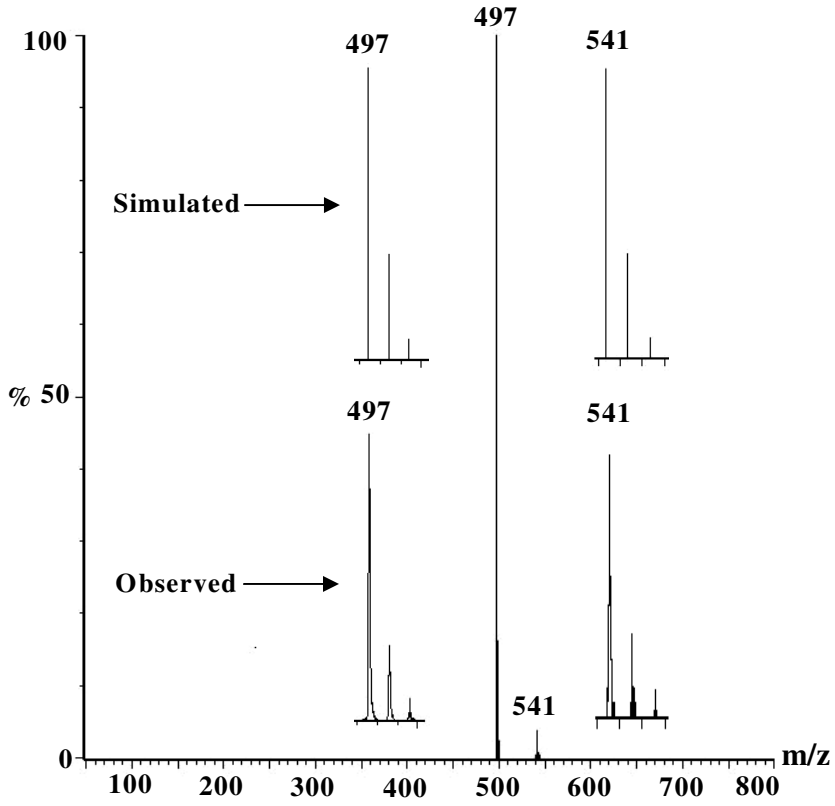

Fig. S2 Electrospray ionization mass spectrum positive (ESI-MS positive) of $[Cd_2L(\mu\text{-}H_2O)(H_2O)_2](NO_3)_2{\cdot}4H_2O$ (**2**) in acetonitrile, showing observed and simulated isotopic distribution patterns.

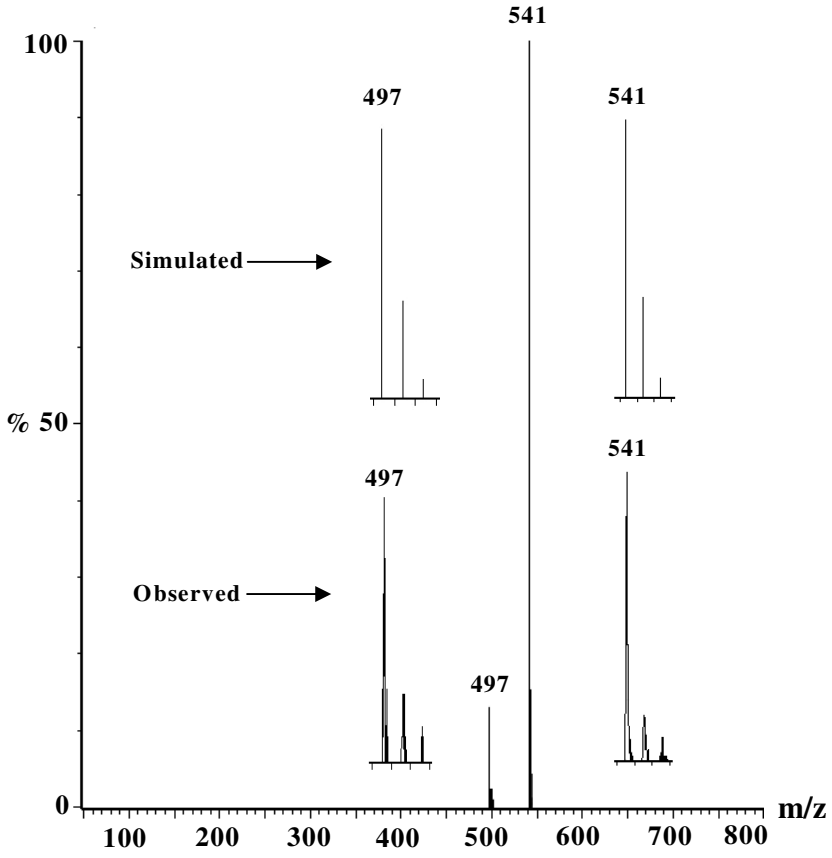

Fig. S3 Electrospray ionization mass spectrum positive (ESI-MS positive) of $[Hg_2LCl_2]$ (**3**) in acetonitrile, showing observed and simulated isotopic distribution patterns.

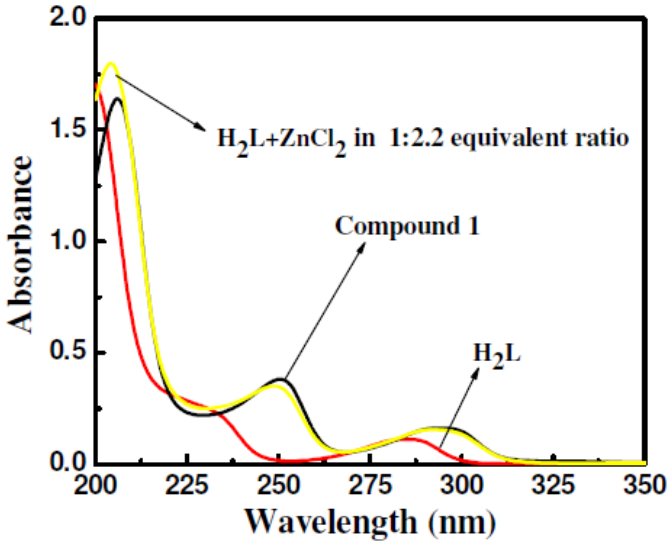

Fig. S4 UV-Vis spectra of H_2L (2×10^{-5} M), $[Zn_2LCl_2]\cdot 2CH_3OH$ (**1**) (2×10^{-5} M) and solution of H_2L+$ZnCl_2$ in 1:2.2 equivalent ratio in acetonitrile.

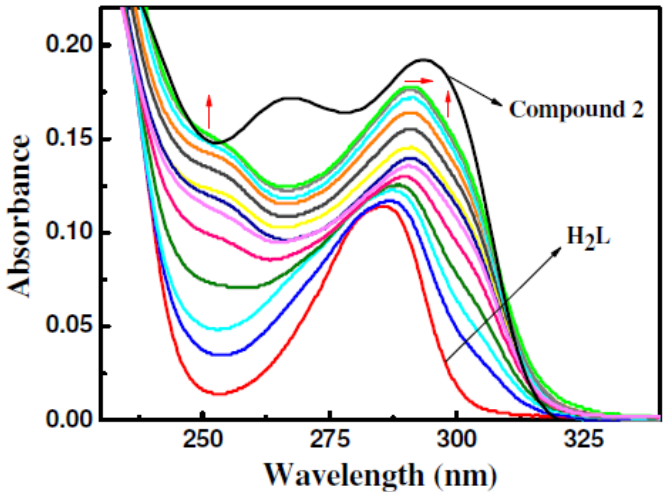

Fig. S5 Spectrophotometric titration of H_2L (2×10^{-5} M) with $Cd(NO_3)_2\cdot 4H_2O$ (0–2.6 equiv) in acetonitrile.

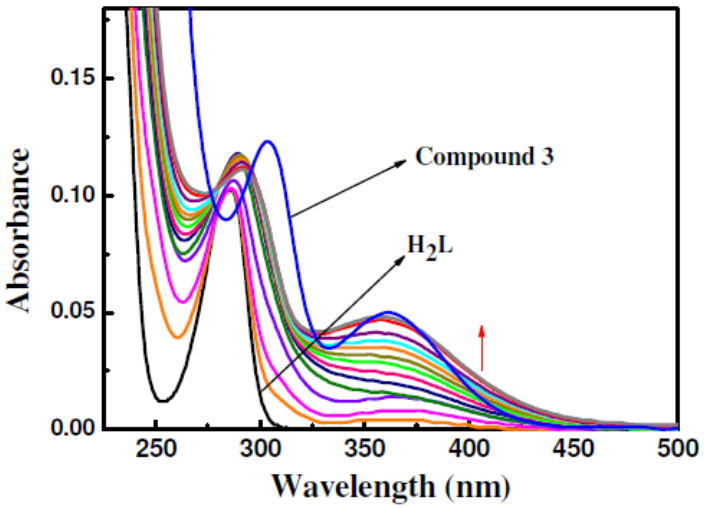

Fig. S6 Spectrophotometric titration of the H_2L (2×10^{-5} M) with {$Hg(NO_3)_2 \cdot H_2O$ + NaCl} (0–2.6 equiv) in methanol–H_2O–acetonitrile (1:1:50).

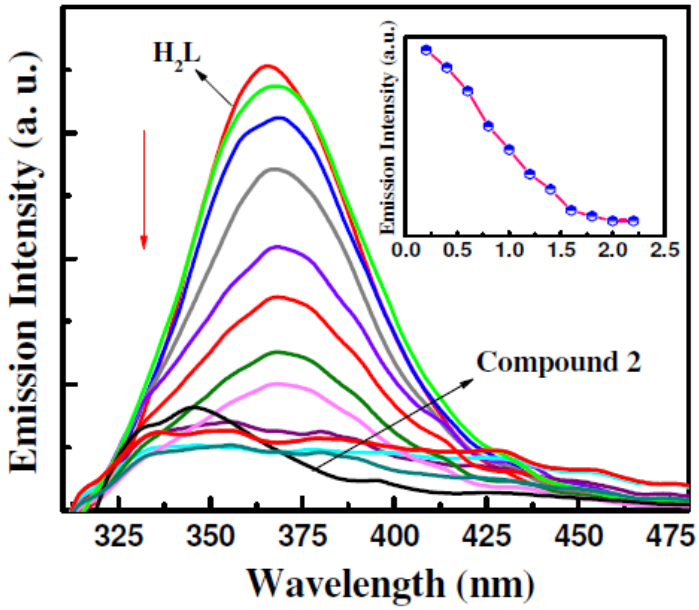

Fig. S7 Spectrofluorimetric titration of H_2L (2×10^{-5} M) with $Cd(NO_3)_2 \cdot 4H_2O$ in acetonitrile. The arrow indicates the increasing concentration of $Cd(NO_3)_2 \cdot 4H_2O$ added. The inset shows the variation of the emission intensity with number of equivalents of $Cd(NO_3)_2 \cdot 4H_2O$ added. λ_{ex} = 286 nm.

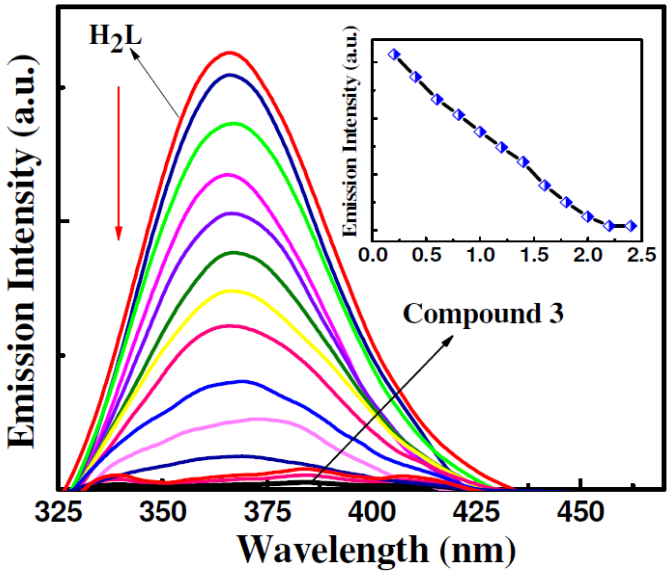

Fig. S8 Spectrofluorimetric titration of H_2L (2×10^{-5} M) with $Hg(OAc)_2$ in methanol–acetonitrile (1:50). The arrow indicates the increasing concentration of $Hg(OAc)_2$ added. The inset shows the variation of the emission intensity with number of equivalents of $Hg(OAc)_2$ added. λ_{ex} = 286 nm.

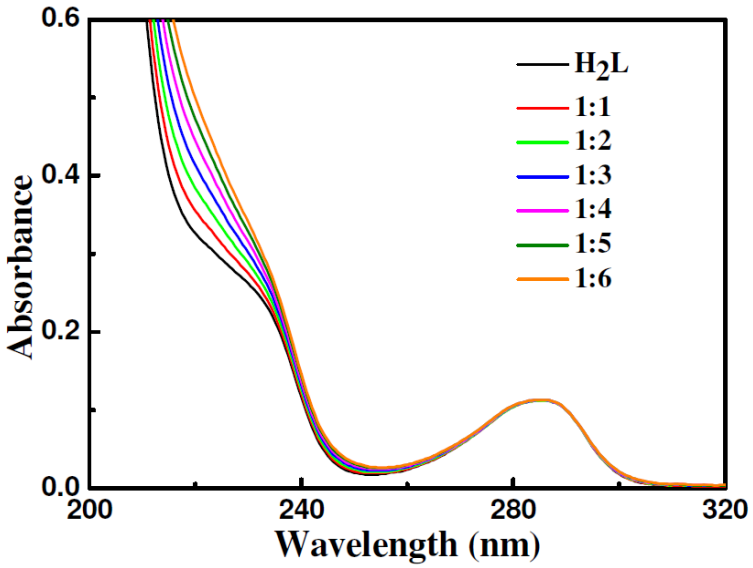

Fig. S9 Spectrophotometric titration of H_2L (2×10^{-5} M) with triethylamine in acetonitrile.

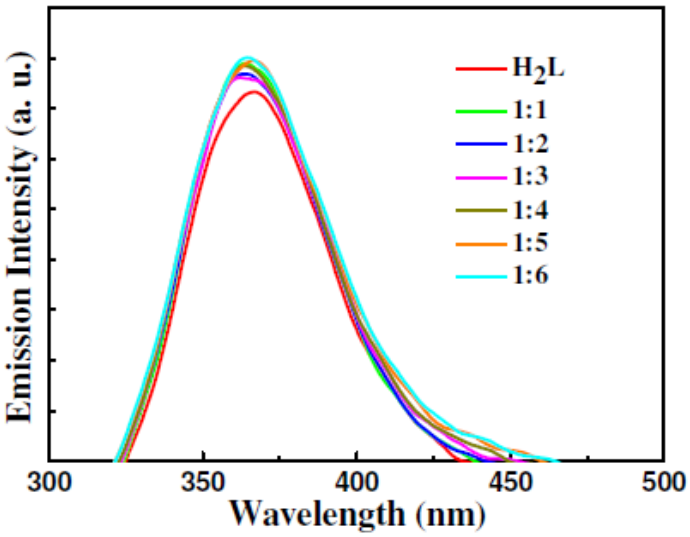

Fig. S10 Spectrofluorimetric titration of H_2L (2×10^{-5} M) with triethylamine in acetonitrile. λ_{ex} = 286 nm.

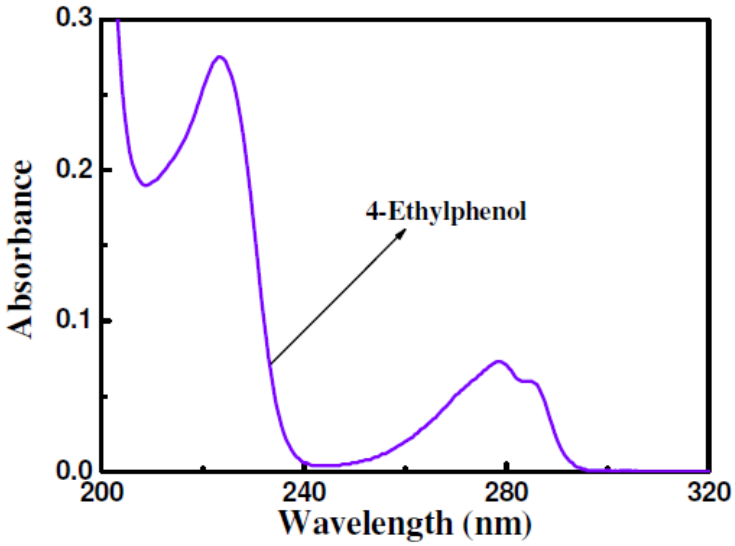

Fig. S11 UV-Vis spectrum of 4-ethylphenol (4×10^{-5} M) in acetonitrile.

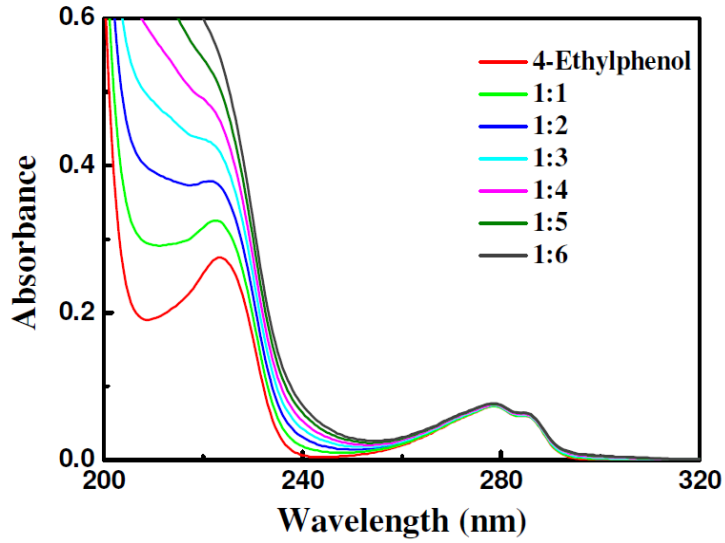

Fig. S12 Spectrophotometric titration of 4-ethylphenol (4×10^{-5} M) with triethylamine in acetonitrile.

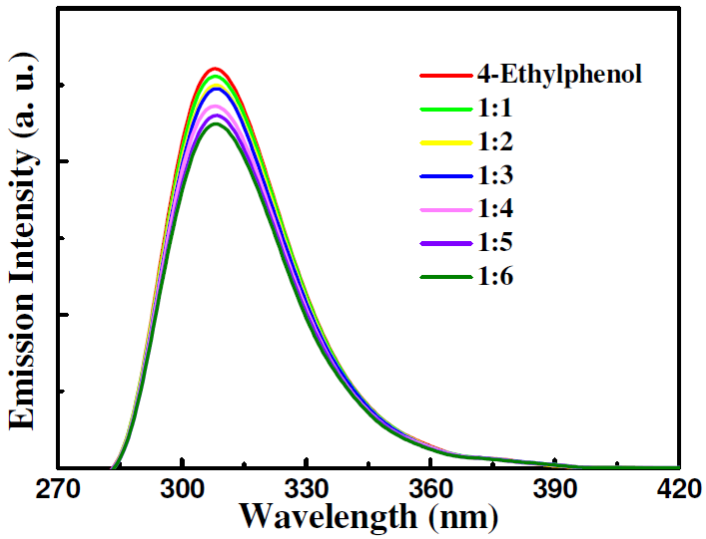

Fig. S13 Spectrofluorimetric titration of 4-ethylphenol (4×10^{-5} M) with triethylamine in acetonitrile. λ_{ex} = 278 nm.

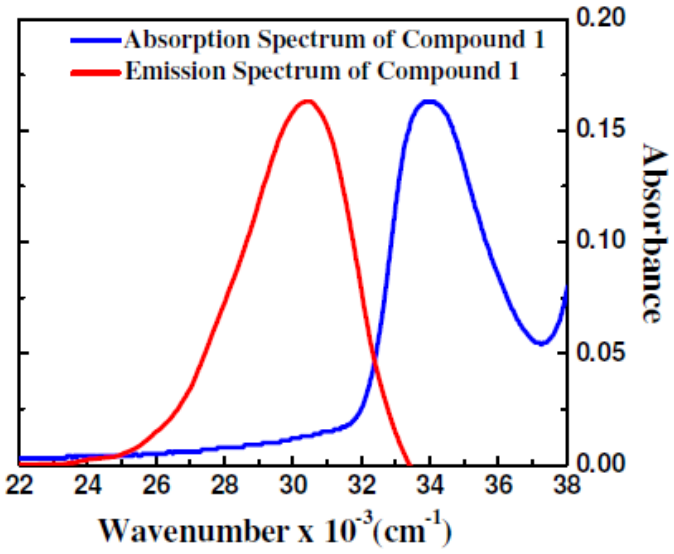

Fig. S14 Lowest energy absorption band and fluorescence spectra of the dizinc(II) compound **1**, revealing closely mirror image relationship.

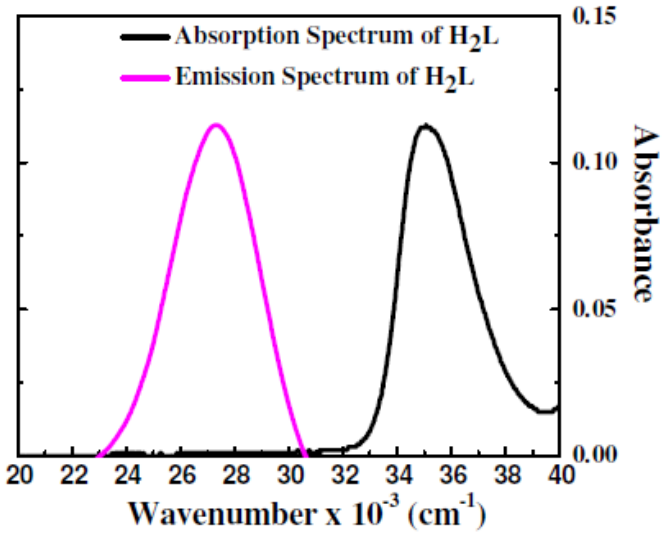

Fig. S15 Lowest energy absorption band and fluorescence spectra of H_2L, revealing that there is no mirror image relationship.

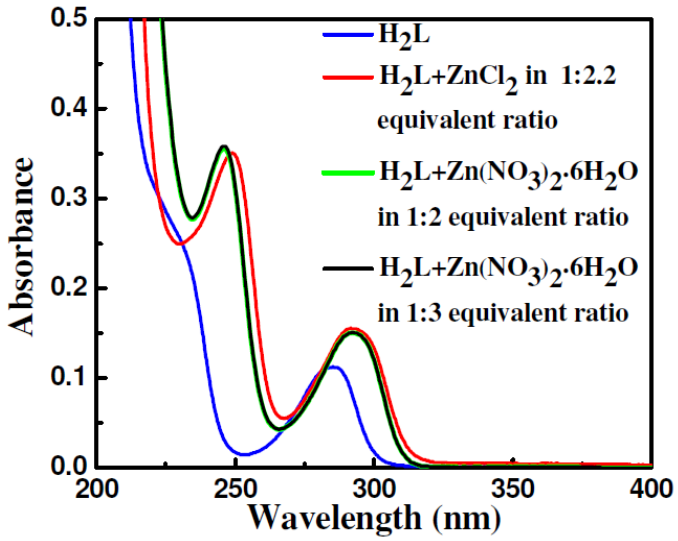

Fig. S16 Comparative UV-Vis spectra of H_2L, 1:2.2 (saturated) H_2L–$ZnCl_2$ and 1:2 and 1:3 (both saturated) H_2L–$Zn(NO_3)_2.6H_2O$ in acetonitrile. Concentration of H_2L: 2×10^{-5} M.

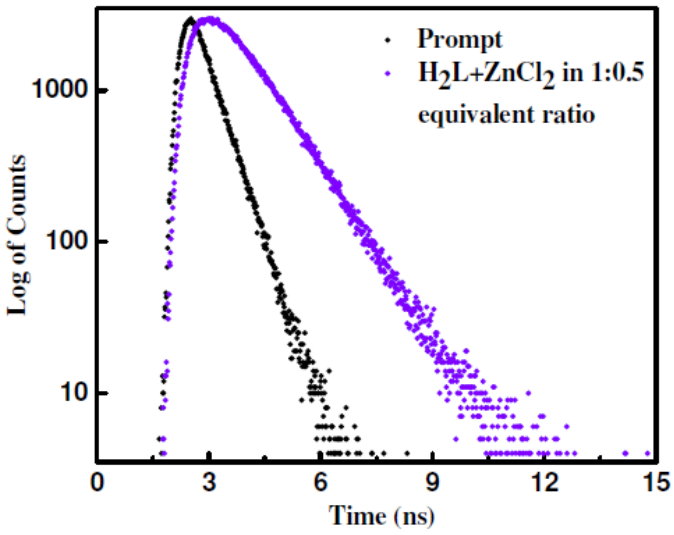

Fig. S17 Time-resolved fluorescence decay of 1:0.5 equivalent mixture of H_2L (2×10^{-5} M) and $ZnCl_2$ in acetonitrile. The fluorescence was monitored at 330 nm.

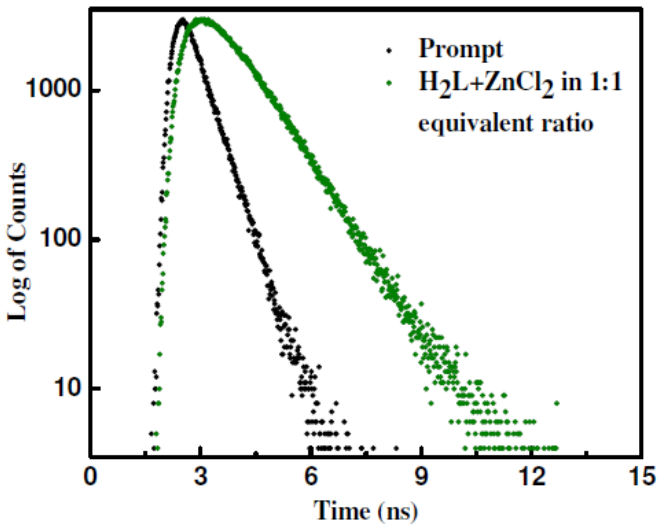

Fig. S18 Time-resolved fluorescence decay of 1:1 equivalent mixture of H_2L (2×10^{-5} M) and $ZnCl_2$ in acetonitrile. The fluorescence was monitored at 330 nm.

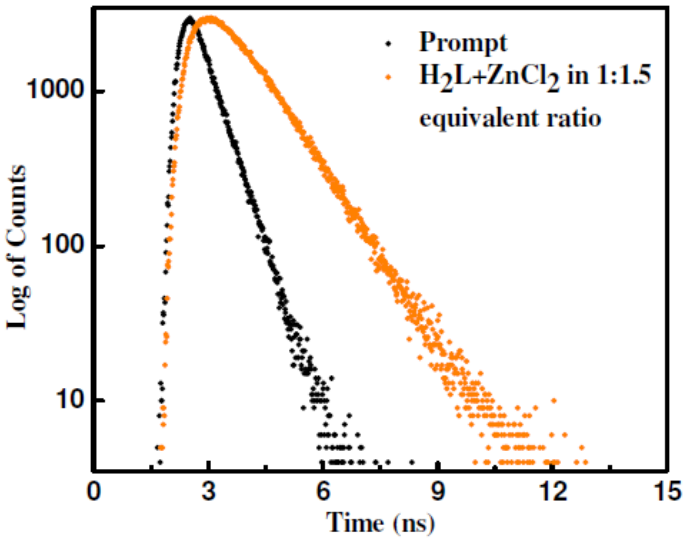

Fig. S19 Time-resolved fluorescence decay of 1:1.5 equivalent mixture of H_2L (2×10^{-5} M) and $ZnCl_2$ in acetonitrile. The fluorescence was monitored at 330 nm.

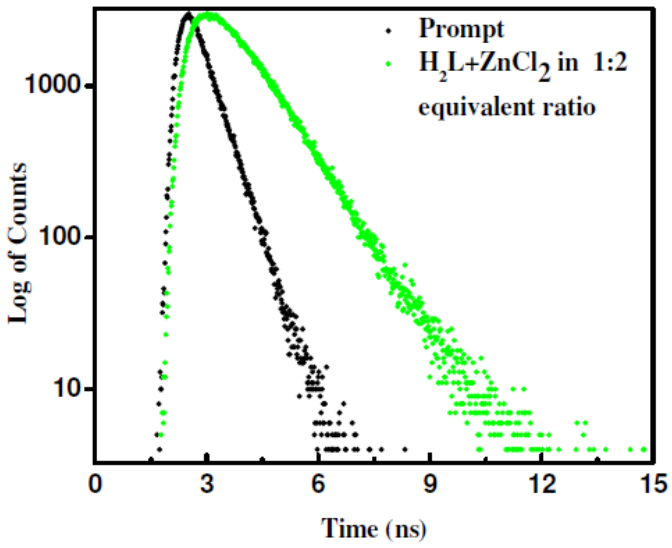

Fig. S20 Time-resolved fluorescence decay of 1:2.0 equivalent mixture of H_2L (2×10^{-5} M) and $ZnCl_2$ in acetonitrile. The fluorescence was monitored at 330 nm.

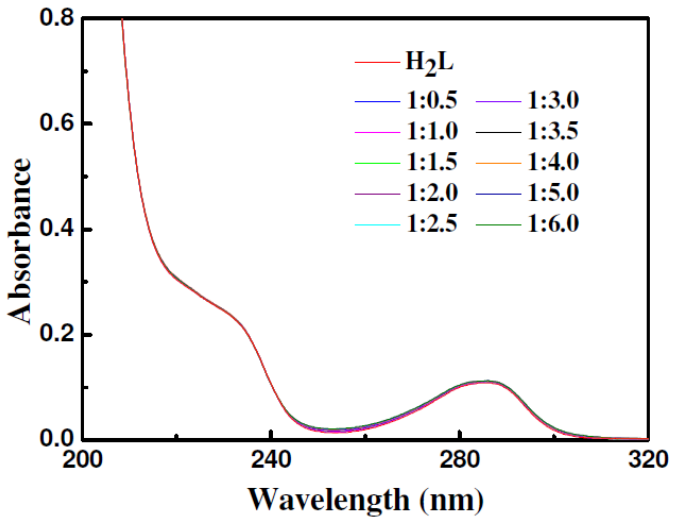

Fig. S21 Spectrophotometric titration of H_2L (2×10^{-5} M) with acetic acid in acetonitrile.

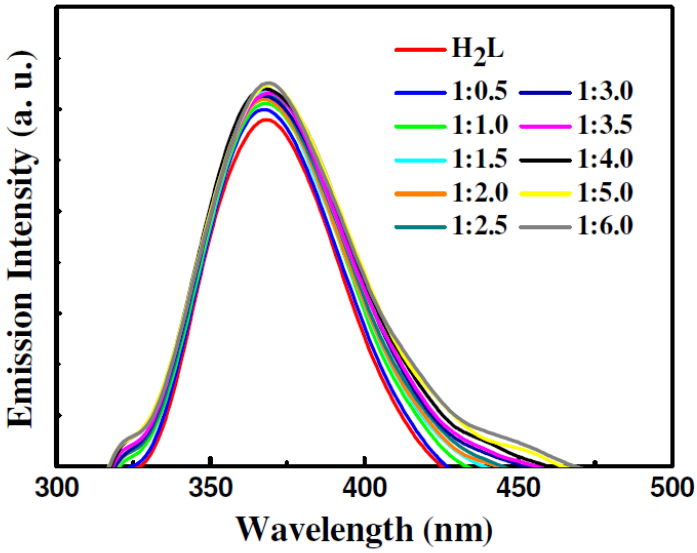

Fig. S22 Spectrofluorimetric titration of H_2L (2×10^{-5} M) with acetic acid in acetonitrile. λ_{ex} = 286 nm.

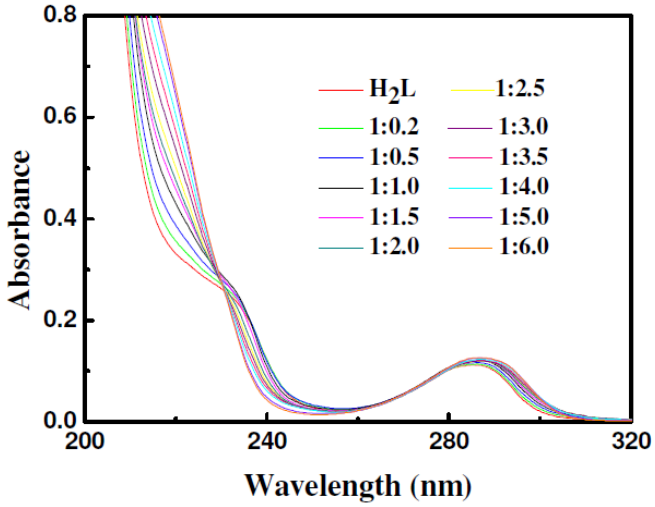

Fig. S23 Spectrophotometric titration of H_2L (2×10^{-5} M) with nitric acid in 1:30 water-acetonitrile.

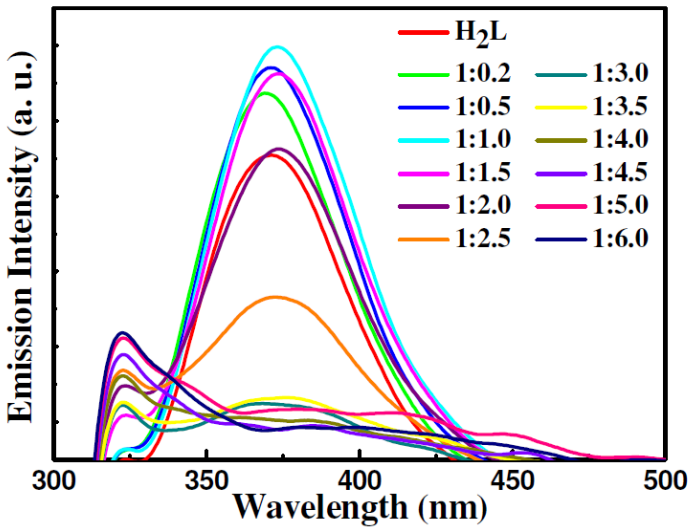

Fig. S24 Spectrofluorimetric titration of H_2L (2×10^{-5} M) with nitric acid in 1:30 water-acetonitrile. λ_{ex} = 286 nm.

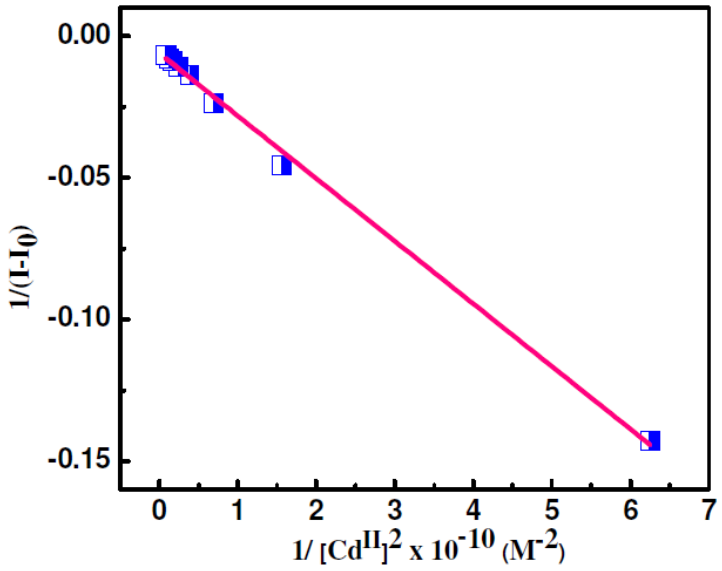

Fig. S25 Benesi–Hildebrand plot for the titration of H_2L with $Cd(NO_3)_2{\cdot}4H_2O$ in acetonitrile.

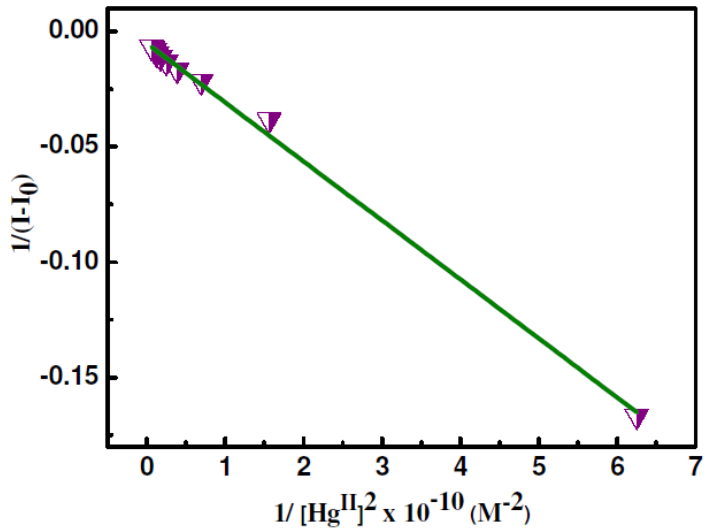

Fig. S26 Benesi–Hildebrand plot for the titration of H_2L (2×10^{-5} M) with $Hg(OAc)_2$ in methanol–acetonitrile (1:50).

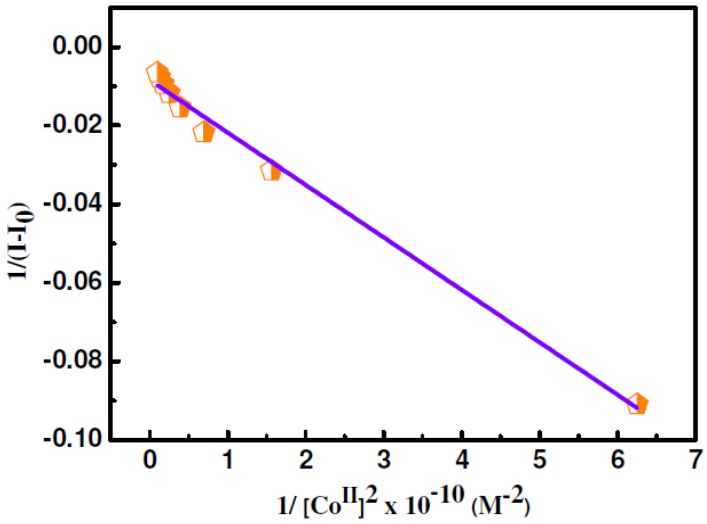

Fig. S27 Benesi–Hildebrand plot for the titration of H_2L (2×10^{-5} M) with $CoCl_2 \cdot 6H_2O$ in acetonitrile.

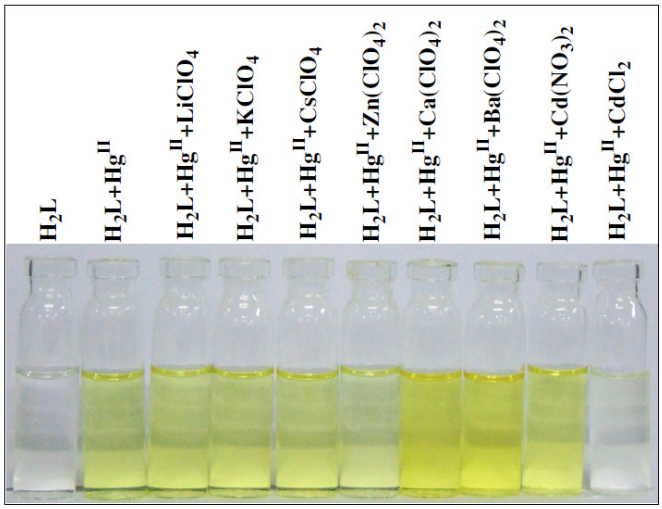

Fig. S28 Colors of H_2L, 1:2 H_2L–$Hg^{II}(OAc)_2$ and 1:2:2 H_2L–$Hg^{II}(OAc)_2$–second metal salt solutions. Concentration of H_2L: 4×10^{-3} M. The solvents are acetonitrile / 1:50 methanol–acetonitrile / 1:1:50 methanol–water–acetonitrile.

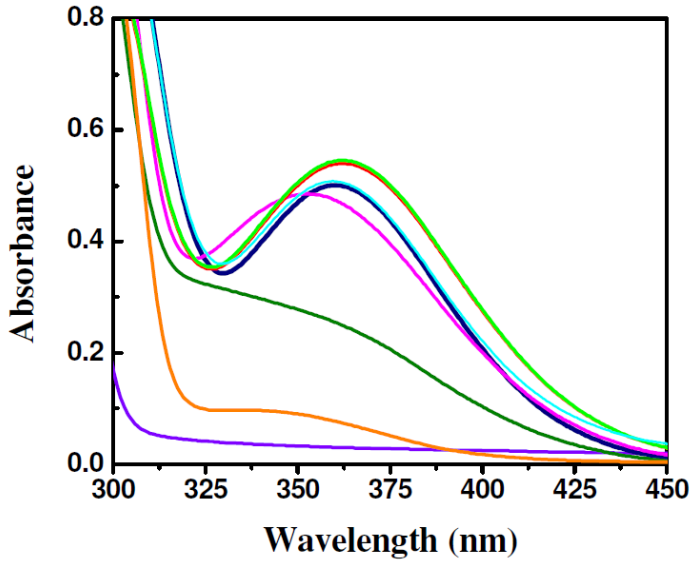

Fig. S29 Parts of the UV-Vis spectra of the solution of H_2L (Violet), 1:2 solution of H_2L and $Hg(OAc)_2$ (Navy) and 1:2:2 solutions of H_2L, $Hg(OAc)_2$ and the following second metal salts: $KClO_4$ (Cyan), $Ca(ClO_4)_2{\cdot}4H_2O$ (Green), $Ba(ClO_4)_2{\cdot}H_2O$ (Red), $Zn(ClO_4)_2{\cdot}6H_2O$ (Olive), $Cd(NO_3)_2{\cdot}4H_2O$ (Magenta) and $CdCl_2{\cdot}H_2O$ (Orange). Concentration of H_2L: 1.5×10^{-4} M. The solvents are acetonitrile / 1:50 methanol-acetonitrile / 1:1:50 methanol-water-acetonitrile.